

Polar growth in the Alphaproteobacterial order Rhizobiales

Pamela J. B. Brown^a, Miguel A. de Pedro^b, David T. Kysela^a, Charles Van der Henst^c, Jinwoo Kim^{a,1}, Xavier De Bolle^c, Clay Fuqua^a, and Yves V. Brun^{a,2}

^aDepartment of Biology, Indiana University, Bloomington, IN 47405; ^bCentro de Biología Molecular Severo Ochoa, Consejo Superior de Investigaciones Científicas, Universidad Autónoma de Madrid, Campus de Cantoblanco, 28049 Madrid, Spain; and ^cResearch Unit in Molecular Biology, Department of Biology, University of Namur, Facultés Universitaires Notre-Dame de la Paix, 5000 Namur, Belgium

Edited* by Eugene W. Nester, University of Washington, Seattle, WA, and approved December 8, 2011 (received for review September 2, 2011)

Elongation of many rod-shaped bacteria occurs by peptidoglycan synthesis at discrete foci along the sidewall of the cells. However, within the Rhizobiales, there are many budding bacteria, in which new cell growth is constrained to a specific region. The phylogeny of the Rhizobiales indicates that this mode of zonal growth may be ancestral. We demonstrate that the rod-shaped bacterium *Agrobacterium tumefaciens* grows unidirectionally from the new pole generated after cell division and has an atypical peptidoglycan composition. Polar growth occurs under all conditions tested, including when cells are attached to a plant root and under conditions that induce virulence. Finally, we show that polar growth also occurs in the closely related bacteria *Sinorhizobium meliloti*, *Brucella abortus*, and *Ochrobactrum anthropi*. We find that unipolar growth is an ancestral and conserved trait among the Rhizobiales, which includes important mutualists and pathogens of plants and animals.

cell wall morphogenesis | cell elongation-division cycle

Elongation of most rod-shaped bacterial cells is thought to be mediated by peptidoglycan synthesis along the sidewall of the cells and depends on the elongase, a protein complex consisting of MreBCD, RodA, and PBP2 [reviewed (1)]. Peptidoglycan synthesis continues laterally until a cell has roughly doubled in length, at which point new cell wall precursors are directed to the division site by the bacterial tubulin homolog FtsZ (2). After completion of cell division, peptidoglycan biosynthesis is redirected to lateral growth along the sidewall.

Although these modes of cell growth are generally thought to be predominant among rod-shaped bacteria, in Actinobacteria, elongation occurs at the cell poles and requires the polarity determinant protein DivIVA (3–8). In addition, a striking type of polar growth is found within some Alphaproteobacteria that grow by budding (9) (Fig. 1*A*). In budding bacteria, new daughter cells emerge strictly from the pole of the mother cell. Thus, we presume that new cell wall synthesis must be restricted to a small polar area. The scattered distribution of budding bacteria within the Rhizobiales (Fig. 1*A*) suggests an ancestral origin of budding, indicating that members of the *Rhizobiaceae* and *Brucellaceae* families may also grow by polar extension rather than their usually assumed dispersed mode of growth. Further support for this hypothesis is provided by the observation that mutations or treatments that impair cell division in *Brucella abortus* (10, 11), *Sinorhizobium meliloti* (12, 13), and *Agrobacterium tumefaciens* (14–18) cause branching morphologies to arise, rather than filamentation. Finally, the genomes of bacteria belonging to the *Rhizobiaceae* and *Brucellaceae* families lack known modulators of cell elongation, including a single gene cluster encoding the elongase proteins MreBCD, RodA, and PBP2, suggesting that cell growth may proceed via an alternative mechanism (19, 20).

Results and Discussion

Polar Growth of *A. tumefaciens*. To determine whether polar growth occurs in the *Rhizobiaceae*, we selected the well-studied

plant pathogen *A. tumefaciens* as a model bacterium. Time-lapse microscopy of individual growing *A. tumefaciens* cells revealed that the cell growth was asymmetric and initiation of constriction occurred at the future site of cell division even in relatively small cells (Fig. 1*B* and *Movie S1*). Transmission electron micrographs showed that the width of the cells at the site of constriction was similar (0.8–0.9 μm) in cells with a daughter cell compartment less than 1 μm in length and narrowed as the daughter cell compartment length increased further (Fig. 1*C* and *D*). Notably, a narrow band of FtsZ (Atu_2086) is observed at the site of early constriction in small cells, suggesting that the formation of the early constriction may require the assembly of the FtsZ ring (Fig. 2*A* and *B*). A band of FtsZ is observed at the mid-cell before the initiation of cell division, and a bright focus of FtsZ is found at the mid-cell of deeply constricted cells (Fig. 2*A*). A small focus of FtsZ persists at the new cell pole for a short period after cell division; however, the polar focus disappears before the formation of the band of FtsZ at the site of early constriction. The position of FtsZ in the constriction appears to remain fixed relative to the old pole as the cell grows, suggesting that new cell growth is largely constrained to the daughter cell compartment (Fig. 2*B* and *Movie S2*). Plotting the position of the constriction (as observed in the transmission electron micrographs) relative to the cell poles indicates that the constriction shifts slightly away from the mother cell pole as the cell nears division (Fig. *S1A*). Tracking the length of the mother cell compartment over time in dividing cells reveals that there is only a small increase in mother cell length after cell division (Fig. *S1 B* and *C*). These data suggest that the size of the mother cell compartment is relatively constant and we infer that new cell growth occurs primarily within the daughter cell compartment.

To identify regions of new cell growth, *A. tumefaciens* cells were pulse labeled with the amine reactive dye Texas red-X succinimidyl ester (TRSE), which stains cell surface proteins. In *E. coli* the signal from TRSE-stained proteins dissipated homogeneously along the sidewalls of the cells as a consequence of lateral cell growth as previously shown (21) but remained trapped at the old cell poles, which are comprised of inert peptidoglycan (Fig. 3*A* and *Movie S3*). In contrast, the fluorescent signal from TRSE remained fixed in *A. tumefaciens* (Fig. 3*B* and *C*, Fig. *S2B*, and *Movies S4*, *S5*, and *S6*), suggesting that the main body of the cells, and not just the poles, were inert. When the

Author contributions: P.J.B.B., M.A.d.P., D.T.K., C.F., and Y.V.B. designed research; P.J.B.B., M.A.d.P., D.T.K., C.V.d.H., and J.K. performed research; P.J.B.B. contributed new reagents/analytic tools; P.J.B.B., M.A.d.P., D.T.K., C.V.d.H., J.K., X.D.B., C.F., and Y.V.B. analyzed data; and P.J.B.B., M.A.d.P., C.F., and Y.V.B. wrote the paper.

The authors declare no conflict of interest.

*This Direct Submission article had a prearranged editor.

¹Present address: Department of Applied Biology, Gyeongsang National University, Jinju 660-701, Korea.

²To whom correspondence should be addressed. E-mail: ybrun@indiana.edu.

This article contains supporting information online at www.pnas.org/lookup/suppl/doi:10.1073/pnas.1114476109/-DCSupplemental.

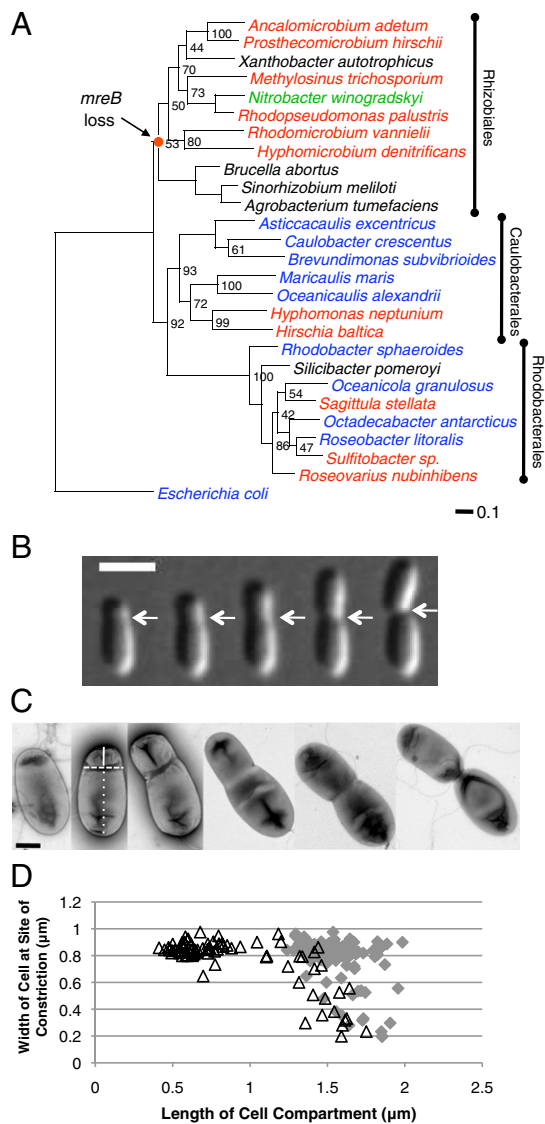


Fig. 1. Phylogeny and morphology of *A. tumefaciens* are suggestive of polar growth. (A) Maximum likelihood phylogeny inferred from *gyrA* sequences. Taxon label colors indicate bacteria described as reproducing by budding (red), binary fission (blue), budding or binary fission (green), and bacteria for which the mode of reproduction is not clearly described (black) (40). Node values indicate clade frequency among 100 nonparametric bootstrapped datasets. The scale bar indicates the estimated number of substitutions per site. The node where *mreB* (and the associated *mreCD*, *rodA*, *pbpB* genes) is predicted to have been lost within the Rhizobiales is indicated. See *SI Materials and Methods* for details of phylogenetic reconstruction. (B) Time-lapse microscopy of a single *A. tumefaciens* cell reveals that constriction of *A. tumefaciens* cells occurs before cell division. White arrows indicate the site of constriction. Images shown were taken at 30-min intervals. (Scale bar: 2 μm .) (C) Transmission electron micrographs of individual *A. tumefaciens* cells at different stages in the cell cycle. The lines in the second panel illustrate metrics used in quantification. Solid line is length of daughter cell compartment, dashed line is the width of the cell at the site of constriction, and dotted line is the length of the mother cell compartment. (Scale bar: 0.5 μm .) (D) Width of cells at the site of constriction is plotted against the length of the daughter cell compartment (open black triangles) and length of the mother cell compartment (gray diamonds).

growth of a fully stained newborn cell was tracked, unlabeled regions generated by the insertion of new surface protein emerged exclusively from one end of the cell (Fig. 3B and Movie S4). Furthermore, while bands of FtsZ-eGFP are readily observed in

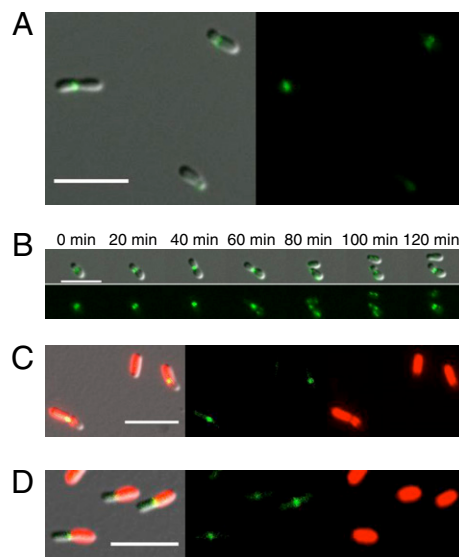


Fig. 2. FtsZ-eGFP localizes to the early constriction in *A. tumefaciens*. (A) FtsZ-eGFP localization in wild type *A. tumefaciens*. (B) Time-lapse microscopy of a single *A. tumefaciens* cell expressing FtsZ-eGFP during growth. (C) FtsZ-eGFP localization in TRSE-stained *A. tumefaciens* cells after a short (15-min) chase. (D) FtsZ-eGFP localization in TRSE-stained *A. tumefaciens* cells after a longer (2-h) chase.

the regions stained with TRSE after a short chase (15 min; Fig. 2C), after a chase long enough to allow cell division (2 h), the bands of FtsZ-eGFP are consistently observed at the junction of the new and old cell material (Fig. 2D). This observation suggests that the junction between new and old cell material constitutes the future site of cell division. We conclude that cell growth is constrained to the daughter cell compartment.

To precisely determine the region of active growth, we observed older cells pulse labeled with TRSE. If cell growth occurs at the cell pole, the TRSE should remain fixed within the daughter cell compartment; however, if growth occurs at the junction between the mother and daughter cell compartments, TRSE should persist at both cell poles (Fig. S24). TRSE remained fixed in the daughter cell compartment as the cells grew, indicating that new cell growth is not dispersed throughout the daughter cell compartment (Fig. 3C, Fig. S2B, and Movies S5 and S6). An unlabeled region initially emerged from one end of the cell suggesting that elongation occurs at the cell pole and not at the region where the constriction is observed (Fig. S2B and Movie S6). In predivisional cells an unlabeled region was observed at the mid-cell just before cell division (Fig. 3C, 20 min; Fig. S2B, 80 min). The insertion of new material at the mid-cell is likely to be responsible for the modest increase in size observed in the mother cells (Fig. S1C). After cell division, unlabeled material emerged from the newly generated cell poles (Fig. 3C, Fig. S2B, and Movies S5 and S6). We conclude that new outer membrane protein insertion occurs at two distinct regions: the younger cell pole and the mid-cell of predivisional cells.

Similar patterns of TRSE segregation were observed in situ when *A. tumefaciens* cells were pulse labeled with TRSE and grown in association with an *Arabidopsis thaliana* plant root (Fig. S3 and Movies S7, S8, and S9). *A. tumefaciens* is a plant pathogen that can initiate extensive physical and genetic interactions with a wide range of host plants (22). Virulent interactions are stimulated by the presence of plant-released signals, primarily by phenolic lignin precursors such as acetosyringone (23). We therefore examined growth patterns under virulence inducing conditions and in association with plant roots (Fig. S3A–C), and observed that localized insertion of new outer membrane proteins

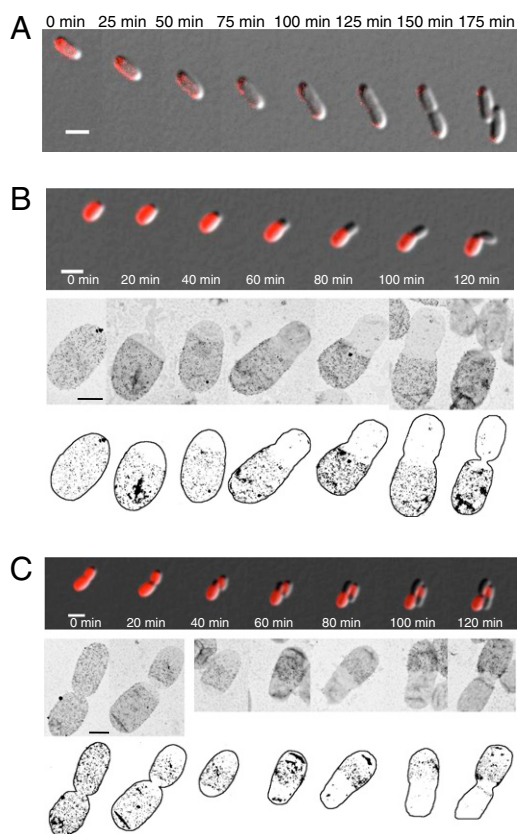


Fig. 3. *A. tumefaciens* cells display zonal cell wall synthesis. (A) Time-lapse microscopy of growth of a single *E. coli* cell pulse labeled with TRSE. (B) Growth pattern of a young cell pulse labeled with TRSE and D-cys labeling patterns of individual cell sacculi. Illustrations of the D-cys-labeled sacculi are provided. (C) Growth pattern of a predivisional cell pulse labeled with TRSE and D-cys-labeling patterns of individual cell sacculi. Illustrations of the D-cys-labeled sacculi are provided. (White scale bars: 2 μm ; black scale bars: 0.5 μm .)

occurs under virulence inducing conditions (Fig. S3A and Movie S7). When *A. tumefaciens* cells are grown under conditions in which nutrients are provided by an *Arabidopsis thaliana* plant root, localized new protein insertion occurs among both attached and unattached cells (Fig. S3B and Movie S8). To ensure that localized protein insertion occurs when cells are attached to the plant root, fluorescent wheat germ agglutinin (WGA) was used to detect the unipolar polysaccharide, an adhesin which is specifically deployed at the point of cell-to-surface contact after initial attachment (24, 25) (Fig. S3C and Movie S9). Notably, these observations indicate that cells preferentially attach to surfaces at the old cell pole.

To determine if the observed regions of new protein insertion are indicative of cell growth due to expansion of the cell wall, D-cysteine (D-cys) labeling was used to monitor peptidoglycan synthesis. D-cys incorporates into peptidoglycan by replacing the terminal D-Ala residue of mucopeptides and can be readily detected immunochemically in purified sacculi (2). After an appropriate chase period, the presence of D-cys in the sacculi demarks regions of old peptidoglycan, whereas unlabeled regions are comprised of newly synthesized peptidoglycan. Elongation of *E. coli* cells by diffuse insertion of new peptidoglycan causes a uniform decrease in the density of the signal from D-cys (2). In *A. tumefaciens*, D-cys incorporated specifically into mucopeptides M4, D44, and T444 and did not adversely affect cell morphology (Table S1 and Fig. S4). Sacculi isolated from cells pulse-labeled with D-cys were comprised of regions either heavily labeled with D-cys or essentially devoid of label (Fig. 3B and C and Fig. S2B).

A variety of D-cys labeling patterns were observed for individual sacculi and were readily correlated with the patterns observed during growth of TRSE-stained cells (Fig. 3B and C and Fig. S2B). Notably, bands of D-cys and TRSE persisted at fixed locations in daughter cells (Fig. 3C, Fig. S2B, and Movies S5 and S6). After a chase period of 3.25 doublings, we observed that 12.7% (23/181) of the sacculi were heavily labeled, consistent with the expected value of 10.5% if the peptidoglycan is essentially inert with little or no turnover (Fig. S2C). In sum, we conclude that: (i) once synthesized, the peptidoglycan is stable; (ii) peptidoglycan synthesis is constrained to the cell pole during elongation; (iii) polar peptidoglycan synthesis is terminated and peptidoglycan synthesis is redirected to the mid-cell of predivisional cells to allow septum formation; and (iv) peptidoglycan synthesis continues at the new cell pole generated after cell division to drive elongation (Fig. 4).

Polar Growth Is Conserved Among the Rhizobiales. Because other members of the *Rhizobiaceae* and *Brucellaceae* families share a tendency to form branches rather than filaments when cell division is blocked (10, 13), and lack known modulators of cell elongation including MreB, the growth patterns of *S. meliloti* (Fig. 5A), *Brucella abortus* (Fig. 5B and Movie S10), and *Ochrobactrum anthropi* (Fig. 5C and Movie S11) were examined. Visualization of D-cys labeled sacculi from *S. meliloti* after a short chase period revealed that peptidoglycan synthesis occurs primarily at the cell pole and also at the mid-cell of predivisional cells in this bacterium (Fig. 5A). Time-lapse microscopy of TRSE stained *B. abortus* and *O. anthropi* revealed that new material emerged strictly from the new cell poles generated after cell division (Fig. 5B and C and Movies S10 and S11). Broadening our analysis to include classically defined budding bacteria within the Rhizobiales, we demonstrate that for *Hyphomicrobium denitrificans* (Fig. 5D) and *Prosthecomicrobium hirschii* (Fig. 5E and Movie S12) new cell material emerged from the cell poles in cells pulse labeled with TRSE. In addition, recent reclassification of described budding bacteria (26–29) indicates that this mode of growth is widespread throughout the Rhizobiales (Fig. 1A and Fig. S5). Thus, we conclude that polar elongation is an ancient trait in the Rhizobiales.

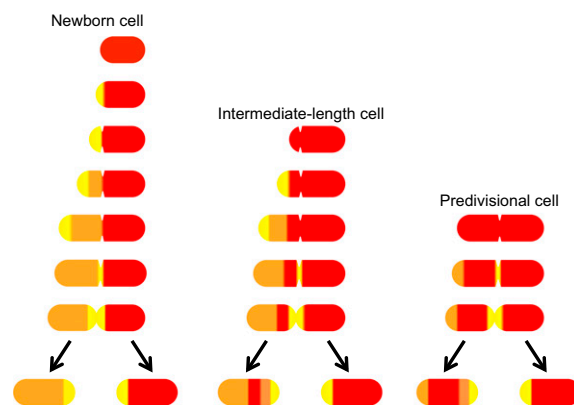


Fig. 4. Model for the segregation of peptidoglycan and outer membrane labels in *A. tumefaciens* cells. The illustration shows the expected patterns for the distribution of labeled peptidoglycan or outer membrane in cells of different ages at the initiation of the chase, as indicated above each panel. Red indicates the area of the cell retaining the original label. Yellow indicate areas of active PG synthesis. Areas of new, unlabeled PG are shown in orange. The location of the label will remain constant in newly generated daughter cells due to the conservative nature of the growth process. The labeling and subsequent growth of intermediate and predivisional cells clearly explains generation of cells (and sacculi) with well-defined thin or thick bands of labeled material, respectively.

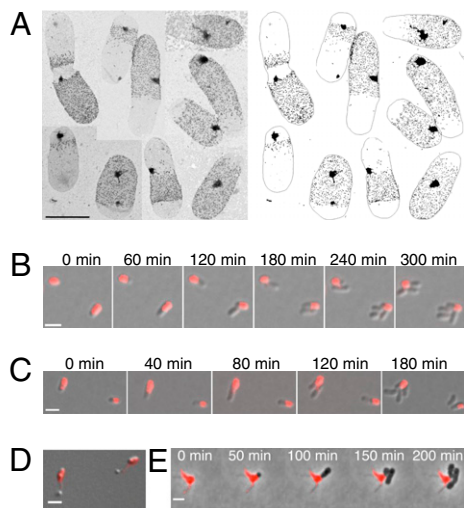


Fig. 5. Unipolar growth is conserved among the Rhizobiales. (A) *d*-cys labeling of individual *S. meliloti* sacculi. (Scale bar: 0.5 μm .) (B) Time-lapse microscopy of TRSE-stained *Brucella abortus* 544 cells. (C) Time-lapse microscopy of TRSE-stained *O. anthropi* cells. (D) TRSE-stained *H. denitrificans* cells after 18 h. (E) Time-lapse microscopy of TRSE-stained *P. hirschii* cells. (White scale bars: 2 μm .)

Peptidoglycan Composition of *A. tumefaciens* and *S. meliloti* is Atypical.

Because polar elongation causes the generation of a high proportion of inert peptidoglycan, *A. tumefaciens* peptidoglycan composition was analyzed in detail (Tables S1–S4 and Figs. S6 and S7). The HPLC pattern for *A. tumefaciens* was rather more complex (Fig. S6) than previously reported using a different HPLC protocol (30). Individual peaks were collected and subjected first to MALDI-TOF mass spectrometry to identify the components eluting at each peak. The structure of the peptidoglycan basic subunit in *A. tumefaciens* is the canonical monomer for Gram-negative bacteria, the disaccharide pentapeptide GlucNAc-(β 1 \rightarrow 4)-MurNAc-(L)-Ala-(D)-Glu (γ)-meso-Dap-(D)-Ala-(D)-Ala (30). We identified a total of 23 components that matched the molecular masses expected for muropeptides derived from the canonical monomer by means of known reactions (Table S1). In total, \sim 85% of the total area in the HPLC could be assigned to specific muropeptides. The proposed structures were confirmed by electrospray-MS/MS analysis in all but four minor muropeptides, where ambiguities in the precise position of certain residues could not be resolved (Table S1 and Fig. S7).

A number of notable features differentiate the muropeptide profile of *A. tumefaciens* peptidoglycan from that of *E. coli* (31, 32). First, there was a high abundance of muropeptides cross-linked by LD-Dap-Dap peptide bridges (Tables S2–S4). LD-transpeptidation is not required for incorporation of new peptidoglycan precursors, indicating that postinsertional processing of peptidoglycan likely occurs. Second, anhydro muropeptides, which occupy the C-1 glycan strand terminal position in the peptidoglycan of all characterized Gram-negative bacteria (33), were not detected, suggesting either that *A. tumefaciens* glycan chains are terminated by an unexplained mechanism or the glycan chains are exceptionally long (250–500 disaccharides/chain). Third, we detected the presence of a Dap-Gly-Dap peptide bridge (see muropeptide 8; Fig. S7), a feature which is previously unreported among Gram-negative bacteria. Moreover, *A. tumefaciens* peptidoglycan is highly crosslinked (\sim 64%) due at least in part to accumulation of cross-linked trimers (Table S4). Fourth, the partial amidation of *D*-Glu results in the formation of two muropeptides (see muropeptides 17 and 19; Fig. S7) with Gln

instead of Glu at position 2 in the peptidoglycan stem peptide, constituting another unique structural trait of *A. tumefaciens* peptidoglycan. Lastly, there are no lipoproteins covalently bound to peptidoglycan. An absence of Braun's lipoprotein was also reported for the peptidoglycan of *C. crescentus* suggesting that this may be a feature common to the Alphaproteobacteria (34). Interestingly, analysis of the muropeptide composition of *S. meliloti* peptidoglycan reveals a striking similarity to that of *A. tumefaciens* (Tables S2–S4 and Fig. S6). We infer that the peptidoglycan biosynthesis pathway contains unique features that contribute to or are a consequence of polar growth.

What selective forces have driven the ancient emergence and persistence of such highly localized, polar growth among the Rhizobiales? It is possible to surmise several potential benefits for polar growth. First, recent studies have revealed bacterial aging based on asymmetric inheritance of cellular damage (35, 36). Polar peptidoglycan growth may facilitate reproductive asymmetry by helping to anchor damaged material to the aging mother cell. Second, given the vast number of proteins and coordinated activities required for peptidoglycan synthesis, constraining growth to a single region may prove to be energetically favorable. Lastly, ensuring that the newborn cells are comprised of newly synthesized peptidoglycan and outer membrane proteins may confer an advantage in the case of phase variation by allowing rapid and stable modification of newly synthesized outer membrane proteins and lipids, a trait likely to be exploited by pathogens to avoid detection by the immune systems of their hosts. We note that polar growth also occurs in other bacterial groups including the Caulobacterales (Fig. 1A), Actinobacteria (3, 19, 37), and Planctomycetes (38), suggesting that polar growth may be broadly distributed in bacteria. Therefore, polar growth may provide a target for the development of antibacterial strategies.

Materials and Methods

Strains and growth conditions are described in *SI Materials and Methods*. *D*-cys labeling was performed as previously described (39) with modifications described in *SI Materials and Methods*. The TRSE staining protocol was modified to allow time-lapse microscopy of individual growing cells (21). Briefly, *A. tumefaciens* cells were grown to exponential phase and washed three times in 0.1 M NaHCO_3 , pH 8.3 buffer by centrifugation for 5 min at $5,000 \times g$. Washed cell pellets were resuspended in 200 μL of buffer and TRSE was added to a final concentration of 0.1 $\mu\text{g}/\text{mL}$. Cells were incubated in the dark for 5–10 min. Cells were spotted on an agarose pad immediately after staining and observed using time-lapse microscopy (see *SI Materials and Methods*). A similar TRSE-staining protocol was followed for all bacteria used in this study (see *SI Materials and Methods*). Peptidoglycan purification was performed by a modification of the boiling SDS extraction method (32) as described in the *SI Materials and Methods*. Phylogenetic trees were constructed using either *gyrA* or 16S rRNA sequences from representative species as described in *SI Materials and Methods*.

ACKNOWLEDGMENTS. We thank Daniel Kearns, Patrick Curtis, Gail Hardy, Jason Heindl, and Velocity Hughes for critical reading of this manuscript. Y.V.B. was funded by National Institutes of Health Grants GM051986 and GM077648 and by National Science Foundation Grant MCB0731950. C.F. was funded by National Institutes of Health Grant GM080546. This work was supported by a grant from the Indiana University Metabolomics and Cytomics Initiative (METACyt) program, which is funded, in part, by a major endowment from the Lilly Foundation. P.J.B.B. and D.T.K. were supported by National Institutes of Health National Research Service Awards AI072992 and GM083581, respectively. J.K. was supported by Korean Research Foundation Fellowship KRF-2007-357-F00002. M.A.P. was supported by Ministry of Education and Science, Spain (MEC, BFU2006-04574) and Fundación Ramón Areces. The support of the proteomics department at the Centro de Biología Molecular Severo Ochoa, in particular M. del Valle, is greatly appreciated. C.V.d.H. was supported by a FRIA (Fonds pour la Formation à la Recherche dans l'Industrie et dans l'Agriculture) doctoral fellowship from FRS-FNRS (Fonds de la Recherche Scientifique—Fonds National de la Recherche Scientifique). X.D.B. was funded by FRFC (Fonds de la Recherche Fondamentale Collective Grant 2.4.541.08 from FRS-FNRS) and the University of Namur [Facultés Universitaires Notre-Dame de la Paix (FUNDP)].

1. den Blaauwen T, de Pedro MA, Nguyen-Distèche M, Ayala JA (2008) Morphogenesis of rod-shaped sacculi. *FEMS Microbiol Rev* 32:321–344.
2. de Pedro MA, Quintela JC, Höltje JV, Schwarz H (1997) Murein segregation in *Escherichia coli*. *J Bacteriol* 179:2823–2834.
3. Chauhan A, et al. (2006) Interference of *Mycobacterium tuberculosis* cell division by Rv2719c, a cell wall hydrolase. *Mol Microbiol* 62:132–147.
4. Flårdh K (2003) Essential role of DivIVA in polar growth and morphogenesis in *Streptomyces coelicolor* A3(2). *Mol Microbiol* 49:1523–1536.
5. Kang CM, Nyayapathy S, Lee JY, Suh JW, Husson RN (2008) Wag31, a homologue of the cell division protein DivIVA, regulates growth, morphology and polar cell wall synthesis in mycobacteria. *Microbiology* 154:725–735.
6. Letek M, et al. (2008) DivIVA is required for polar growth in the MreB-lacking rod-shaped actinomycete *Corynebacterium glutamicum*. *J Bacteriol* 190:3283–3292.
7. Nguyen L, et al. (2007) Antigen 84, an effector of pleiomorphism in *Mycobacterium smegmatis*. *J Bacteriol* 189:7896–7910.
8. Ramos A, et al. (2003) Involvement of DivIVA in the morphology of the rod-shaped actinomycete *Brevibacterium lactofermentum*. *Microbiology* 149:3531–3542.
9. Brown PJB, Kysela DT, Brun YV (2011) Polarity and the diversity of growth mechanisms in bacteria. *Semin Cell Dev Biol* 22:790–798.
10. Bellefontaine AF, et al. (2002) Plasticity of a transcriptional regulation network among alpha-proteobacteria is supported by the identification of CtrA targets in *Brucella abortus*. *Mol Microbiol* 43:945–960.
11. Robertson GT, et al. (2000) The *Brucella abortus* CcrM DNA methyltransferase is essential for viability, and its overexpression attenuates intracellular replication in murine macrophages. *J Bacteriol* 182:3482–3489.
12. Cheng J, Sibley CD, Zaheer R, Finan TM (2007) A *Sinorhizobium meliloti* *minE* mutant has an altered morphology and exhibits defects in legume symbiosis. *Microbiology* 153:375–387.
13. Kobayashi H, De Nisco NJ, Chien P, Simmons LA, Walker GC (2009) *Sinorhizobium meliloti* CpdR1 is critical for co-ordinating cell cycle progression and the symbiotic chronic infection. *Mol Microbiol* 73:586–600.
14. Fujiwara T, Fukui S (1972) Isolation of morphological mutants of *Agrobacterium tumefaciens*. *J Bacteriol* 110:743–746.
15. Fujiwara T, Fukui S (1974) Unidirectional growth and branch formation of a morphological mutant, *Agrobacterium tumefaciens*. *J Bacteriol* 120:583–589.
16. Kahng LS, Shapiro L (2001) The CcrM DNA methyltransferase of *Agrobacterium tumefaciens* is essential, and its activity is cell cycle regulated. *J Bacteriol* 183:3065–3075.
17. Su S, Stephens BB, Alexandre G, Farrand SK (2006) Lon protease of the alpha-proteobacterium *Agrobacterium tumefaciens* is required for normal growth, cellular morphology and full virulence. *Microbiology* 152:1197–1207.
18. Latch JN, Margolin W (1997) Generation of buds, swellings, and branches instead of filaments after blocking the cell cycle of *Rhizobium meliloti*. *J Bacteriol* 179:2373–2381.
19. Daniel RA, Errington J (2003) Control of cell morphogenesis in bacteria: Two distinct ways to make a rod-shaped cell. *Cell* 113:767–776.
20. Margolin W (2009) Sculpting the bacterial cell. *Curr Biol* 19:R812–R822.
21. de Pedro MA, Grünfelder CG, Schwarz H (2004) Restricted Mobility of Cell Surface Proteins in the Polar Regions of *Escherichia coli*. *J Bacteriol* 186:2594–2602.
22. Ramey BE, Matthyse AG, Fuqua C (2004) The FNR-type transcriptional regulator SinR controls maturation of *Agrobacterium tumefaciens* biofilms. *Mol Microbiol* 52:1495–1511.
23. Stachel SE, Messens E, Van Montagu M, Zambryski P (1985) Identification of the signal molecules produced by wounded plant cells that activate T-DNA transfer in *Agrobacterium tumefaciens*. *Nature* 318:624–629.
24. Tomlinson AD, Fuqua C (2009) Mechanisms and regulation of polar surface attachment in *Agrobacterium tumefaciens*. *Curr Opin Microbiol* 12:708–714.
25. Li G, et al. (2012) Surface contact stimulates the just-in-time deployment of bacterial adhesins. *Mol Microbiol* 83:41–51.
26. Doronina NV, Trotsenko YA (2003) Reclassification of '*Blastobacter viscosus*' 7d and '*Blastobacter aminooxidans*' 14a as *Xanthobacter viscosus* sp. nov. and *Xanthobacter aminooxidans* sp. nov. *Int J Syst Evol Microbiol* 53:179–182.
27. Kaur J, Verma M, Lal R (2011) *Rhizobium rosettiformans* sp. nov., isolated from a hexachlorocyclohexane dump site, and reclassification of *Blastobacter aggregatus* Hirsch and Muller 1986 as *Rhizobium aggregatum* comb. nov. *Int J Syst Evol Microbiol* 61:1218–1225.
28. van Berkum P, Leibold JM, Eardly BD (2006) Proposal for combining *Bradyrhizobium* spp. (*Aeschynomene indica*) with *Blastobacter denitrificans* and to transfer *Blastobacter denitrificans* (Hirsch and Muller, 1985) to the genus *Bradyrhizobium* as *Bradyrhizobium denitrificans* (comb. nov.). *Syst Appl Microbiol* 29:207–215.
29. Yee B, Oertli GE, Fuerst JA, Staley JT (2010) Reclassification of the polyphyletic genus *Prosthecomicrobium* to form two novel genera, *Vasilyevaea* gen. nov. and *Bauldia* gen. nov. with four new combinations: *Vasilyevaea enhydra* comb. nov., *Vasilyevaea mishustinii* comb. nov., *Bauldia consociata* comb. nov. and *Bauldia litoralis* comb. nov. *Int J Syst Evol Microbiol* 60:2960–2966.
30. Erbs G, et al. (2008) Peptidoglycan and mucopeptides from pathogens *Agrobacterium* and *Xanthomonas* elicit plant innate immunity: Structure and activity. *Chem Biol* 15:438–448.
31. Glauner B (1988) Separation and quantification of mucopeptides with high-performance liquid chromatography. *Anal Biochem* 172:451–464.
32. Glauner B, Höltje JV, Schwarz U (1988) The composition of the murein of *Escherichia coli*. *J Biol Chem* 263:10088–10095.
33. Vollmer W, Blanot D, de Pedro MA (2008) Peptidoglycan structure and architecture. *FEMS Microbiol Rev* 32:149–167.
34. Takacs CN, et al. (2010) MreB drives de novo rod morphogenesis in *Caulobacter crescentus* via remodeling of the cell wall. *J Bacteriol* 192:1671–1684.
35. Lindner AB, Madden R, Demarez A, Stewart EJ, Taddei F (2008) Asymmetric segregation of protein aggregates is associated with cellular aging and rejuvenation. *Proc Natl Acad Sci USA* 105:3076–3081.
36. Stewart EJ, Madden R, Paul G, Taddei F (2005) Aging and death in an organism that reproduces by morphologically symmetric division. *PLoS Biol* 3:e45.
37. Flårdh K (2010) Cell polarity and the control of apical growth in *Streptomyces*. *Curr Opin Microbiol* 13:758–765.
38. Tekniepe BL, Schmidt JM, Starr MP (1982) Immunoferritin labeling shows de novo synthesis of surface components in buds of a prokaryote belonging to mirphototype IV of the *Blastocaulis-Planctomyces* group. *Curr Microbiol* 7:1–6.
39. de Pedro MA, Young KD, Höltje JV, Schwarz H (2003) Branching of *Escherichia coli* cells arises from multiple sites of inert peptidoglycan. *J Bacteriol* 185:1147–1152.
40. Garrity G, et al., eds (2005) *Bergey's Manual of Systematic Bacteriology* (Williams & Wilkins, Baltimore) Vol 2, Part C.

Correction

MICROBIOLOGY

Correction for “Polar growth in the Alphaproteobacterial order Rhizobiales,” by Pamela J. B. Brown, Miguel A. de Pedro, David T. Kysela, Charles Van der Henst, Jinwoo Kim, Xavier De Bolle, Clay Fuqua, and Yves V. Brun, which appeared in issue 5, January 31, 2012, of *Proc Natl Acad Sci USA* (109:1697–1701; first published January 17, 2012; 10.1073/pnas.1114476109).

The authors note that, due to a printer’s error, the affiliation for David T. Kysela should instead appear as Department of Biology, Indiana University, Bloomington, IN 47405. The corrected author and affiliation lines appear below. The online version has been corrected.

**Pamela J. B. Brown^a, Miguel A. de Pedro^b, David T. Kysela^a,
Charles Van der Henst^c, Jinwoo Kim^a, Xavier De Bolle^c,
Clay Fuqua^a, and Yves V. Brun^a**

^aDepartment of Biology, Indiana University, Bloomington, IN 47405; ^bCentro de Biología Molecular Severo Ochoa, Consejo Superior de Investigaciones Científicas, Universidad Autónoma de Madrid, Campus de Cantoblanco, 28049 Madrid, Spain; and ^cResearch Unit in Molecular Biology, Department of Biology, University of Namur, Facultés Universitaires Notre-Dame de la Paix, 5000 Namur, Belgium

www.pnas.org/cgi/doi/10.1073/pnas.1201353109